

# A review of external microbeams for ion beam analyses

L. Giuntini

Received: 31 December 2010 / Revised: 21 February 2011 / Accepted: 8 March 2011 / Published online: 17 April 2011  
© Springer-Verlag 2011

**Abstract** Ion microbeam facilities are analytical tools with high spatial resolution exploiting MeV ion beams. The interactions of beam particles with atoms and nuclei of the target induce the emission of characteristic radiation, the energy of which provides signatures of the compositional and/or structural properties of the target; Ion-Beam Analysis (IBA) techniques, based on the detection of such radiation, enable characterisation of samples of interest, e.g. in material and earth sciences, cultural heritage, biology, medicine, and environmental studies. External beams, obtained by extracting the particles into the atmosphere through a thin window, have many attractive features, e.g. non-destructive/non-invasive analysis and ease of working, so many laboratories have dedicated beam-lines to ex-vacuo IBA analyses. External microprobes have made it possible to obtain probes in the micron range by adopting strong focusing lenses, ultra-thin windows for beam extraction, and short/ultra-short external path of beam particles in light gases; they have also made possible the use of new external IBA techniques, e.g. BS, ERDA, STIM, and IBIC. By adopting systems to raster scan the beam over the sample, imaging capabilities have also become available for ex-vacuo analysis. External scanning microprobes + IBA techniques have enabled the characterisation of samples with high spatial resolution, comparable with that achievable in-vacuum for thick samples, avoiding sample damage.

**Keywords** External microbeam · Ion-Beam Analysis · Ionoluminescence · PIGE · Backscattering Spectrometry · IBIC

## Introduction

Ion microbeam facilities can be seen as analytical tools which, exploiting ion probes with high spatial resolution and energies in the MeV range, provide a rich insight into samples of interest for many fields, for example material and earth sciences, cultural heritage, biology, medicine and environmental studies, by using the wide range of ion-beam analysis (IBA) techniques. These techniques rely on the detection and energy analysis of characteristic radiation emitted by atoms and nuclei of the target when bombarded by MeV ion beams, because the energy of the emitted radiation signatures of the target material. High spatial resolution IBA is most often carried out by using microprobes obtained by the strong focusing action of ion lenses, typically multiplets of magnetic quadrupoles. To fully exploit the potential of a microbeam, ions are raster scanned over the sample, thus enabling the extraction of 2D maps of structural and compositional information from the sample.

Since the early works in the mid of the 1970s [1, 2], the many attractive features of external set-ups, for example the non-destructive and non-invasive character of the analyses and the great ease of working, prompted many laboratories to dedicate beam-lines to IBA for external use. These facilities were oriented to PIXE (Particle Induced X-ray Emission) and PIGE (Particle Induced g-ray Emission) analyses with collimated static milli-beams, the main limitations of which were the restricted number of techniques available, the poor spatial resolution of the probe, and the lack of imaging systems. As reported in the

---

Published in the special issue *Imaging Techniques with Synchrotron Radiation* with Guest Editor Cyril Petibois.

---

L. Giuntini (✉)  
Dipartimento di Fisica dell'Università and Istituto Nazionale di  
Fisica Nucleare, Sezione di Firenze,  
50019, Firenze, Italy  
e-mail: giuntini@fi.infn.it

following, with the advent of external microbeams [3], it has been possible to overcome such limitations. In particular, Backscattering Spectrometry (BS), Elastic Recoil Detection Analysis (ERDA), Scanning Transmission Ion Microscopy (STIM), and Ion Beam Induced Charge (IBIC), scarcely or not used at all with external milli-beam, have also been introduced. Probe dimensions in the micrometer range are normally obtained and scanning systems for the extraction of 2D maps are commonly used.

### Ion microbeam facilities

#### Ion microprobes

Collimated beams constituted the pioneering work in ion microprobe. In what was possibly the first microprobe [4], developed in 1953 for living cell irradiation, a proton beam, with energy up to 1 MeV, was reduced to micrometric size by passing through a pair of optically flat jaws, one of which had a 2.5  $\mu\text{m}$  scratch in the beam direction. It is interesting to note that the beam was then extracted into air through a thin mica window, i.e. *the first microprobe was actually an external microbeam*. Collimated microbeams have several disadvantages, for example:

1. strong reduction of beam intensity [5];
2. relevant particle scattering from the edges of the hole (scattered-to-transmitted beam ratio increases as  $r^{-1}$ ), degrading the aperture itself and both beam energy and dimensions;
3. emission of radiation, limiting in many cases the capabilities of analytical techniques coupled to the microprobe.

For all these reasons the use of collimators to produce microprobes is impractical and is nowadays restricted just to cell ion irradiation (e.g. Refs. [6, 7] and references therein).

The “true” microprobe era dates back to 1970, when Cookson and Pilling, by using a lens made of magnetic quadrupoles, obtained a beam spot of 15  $\mu\text{m}$ , with 15 nA

intensity [5]. Ion beams of MeV energy are significantly more rigid than electrons of a few keV energy, used in electron microprobes (EM), and solenoids, the focusing lenses of EM, are not strong enough to focus such particles, unless superconducting lenses are used [8]. These devices, however, gained little favour because of cost and complexity, liquid helium consumption, and a high stray magnetic field at the target position; as a consequence, magnetic quadrupoles have stood out, because they can exploit the much stronger focusing action of the main component of the magnetic field. The lenses for microprobes are thus commonly made up of quadrupole multiplets (e.g. doublets, Oxford triplet, “Russian” quadruplet, separated quintuplet [9], double doublet with superconducting quadrupoles at the second stage [10], and double triplet [11, 12]), with spatial resolution for IBA measurements down to few hundreds of nanometres, with 50–100 pA intensities (e.g. 290  $\times$  450  $\text{nm}^2$  spot size for a 2 MeV proton beam of 50 pA intensity [13]).

When intermediate or thick samples are to be characterised [14], there is no point in pushing the probe dimensions lower than few microns and most laboratories work with proton beams in the micron range, as the actual dimensions of the probed volume depend not only on the beam dimensions before entering the sample, but also on the “longitudinal resolution” (up to many tens of microns), related to ion penetration inside the sample, and on the “lateral straggling” (up to some microns), because of the interaction with the material of the specimen [15], as depicted in Fig. 1 and summarised in Table 1 for typical energy–particle combinations in light, medium, and heavy targets.

#### Beam scan

Scan systems enable full exploitation of the potential of a microprobe by making possible the collection of 2D maps of structural and compositional properties of the target. This is done by either sweeping the beam over a static target or by moving the target to a fixed beam, the former being by far the most common solution. Its major drawback

**Fig. 1** (a) Zone of interest of the sample and beam spot (top view); (b) beam penetrating into the sample (cross sectional view), investigating a layer thicker than the zone of interest

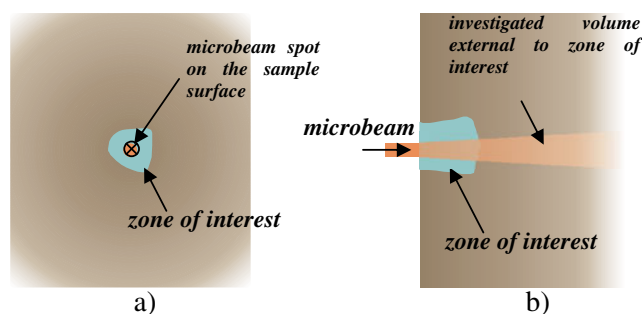


**Table 1** Longitudinal and radial ranges for 2 and 3-MeV alpha particles and 3-MeV protons entering a thick sample of light, medium, heavy atomic weight (TRIM2008 simulation [16])

Energy – particles	Material	Longitudinal range ( $\mu\text{m}$ )		Radial range ( $\mu\text{m}$ )	
		Range	Range straggling	Range	Range straggling
2 MeV – alpha	Mylar	8.5	1.7	3.1	2.1
	Si	7.3	2.6	4.4	3.0
	Iron	3.2	1.6	3.1	2.0
	Gold	2.9	3.0	5.8	3.3
3 MeV – alpha	Mylar	14	1.9	3.8	2.8
	Silicon	12	2.7	5.6	4.0
	Iron	5	1.9	3.7	2.6
	Gold	4.5	3.5	7.2	4.4
3 MeV - proton	Mylar	116	2.0	3.3	3.2
	Silicon	93	2.3	4.4	3.6
	Iron	35	1.2	2.6	2.0
	Gold	27	1.8	4.3	2.7

is the production of aberrations, because of the off-axis entrance of the beam in the lens (in the normally adopted pre-lens configuration), but this is typically a minor effect, if the scan size is within a couple of millimetres.

When larger areas are to be scanned, the target is typically swept under fixed beam, so avoiding aberrations, but fast and repeatable mechanical movements are not trivial to achieve with high degree of accuracy (1  $\mu\text{m}$  or better). In addition, the duration of a full scan, much longer with respect to the time scale of beam current instabilities, may produce inhomogeneities of ion fluence in the scanned area and alterations in the extracted maps. However, by using DC motors and position reading through optical encoders, areas can be scanned at relatively fast speed and full raster scans can be repeated several times over each analysed region, thus averaging the effects of possible current instabilities (see Ref. [17] for references to similar systems). A good example of elemental mapping obtained by raster scanning the sample under a fixed microbeam is reported in Ref. [18]. The sample is on a remotely-controlled stage, equipped with high-precision stepping motors; the mechanical scan enables mapping up to  $1.25 \times 1.25 \text{ cm}^2$ , with a  $3 \text{ mm s}^{-1}$  scanning speed. PIXE maps give information about element migration around inscriptions; in addition, by pointing out the inhomogeneities of the ink over the paper, the extracted maps make evident how the precision and the sensitivity of point analyses are limited by the heterogeneity of the sample nature (paper + ink track), which has to be taken into account for proper comparison of different inks.

A different approach is to combine magnetic and mechanical scanning [19]: the former allows the collection of elemental maps faster than mechanical scanning, within an area up to few  $\text{mm}^2$ , the latter enables collection of a “super map”, composed by all the maps extracted by

magnetic scans; these “super maps” can be as wide as the travel of the mechanical stage range. In Ref. [20] the external scanning microbeam reported in Ref. [19] enabled extraction of maps as wide as many square millimetres and proved to be crucial to clarification of the structure of the painting surface and to understanding the way the great master of Italian Renaissance Antonello da Messina had laid the paint layers to obtain the shading effects, giving also a clear indication of the use of a red lake pigment, not previously acknowledged for the studied portrait.

### External microbeam set-ups

#### Why external set-ups?

In external set-ups, just before (a few millimetres or less) reaching the target, particles are extracted into the atmosphere through a thin window, which has to seal the beam-line and sustain the pressure difference between inside (high vacuum) and outside (atmospheric pressure), though being “transparent” to the beam particles.

An external set-up has many advantages when compared with a conventional arrangement: ease of handling, moving and monitoring the target, no limits to the dimensions of the objects to analyse; no need for sampling; far more effective target heat dissipation; no charging effects; no time-consuming pump-down and refill of the vacuum chamber [21–23]. External beam analysis limits or prevents structural damage, discolouration, drying and outgassing, which may alter samples and/or cause redistribution of elements in the analysed volume (see, e.g., Ref. [24], in which loss of S, Cl, C, and H is reported). In studies of biological samples, external IBA analyses are practically mandatory to reduce organic mass decomposition and enable the study of

living systems (see, e.g., Ref. [25] for an updated list of microbeam facilities for biological applications). External beam analysis has also been used in biomedical applications and on living systems; in the latter case an external set-up is a “*conditio sine qua non*” [26, 27].

Ex vacuo it has been possible to safely characterise delicate works of art, the same studies being impossible or at least hardly feasible in a vacuum, as is confirmed by the many examples reported in the literature, for example analyses of miniature paintings on ancient manuscripts, glazed terracotta, drawings, jewels, embroidery, etc. [28–32].

Beam extraction into the atmosphere requires some caution not to degrade the beam quality. Angular and energy straggling induced by the window and the external path in the atmosphere increase the beam dimensions and broaden the energy distribution of the transmitted particles. As both energy straggling and beam divergence decrease with decreasing crossed areal density  $\rho t$  ( $\rho$  mass density,  $t$  thickness; see, e.g., the Bohr formula for energy straggling and the Molière equation for the scattering angle), the smaller the areal density of the external path (window + atmosphere), the better the external beam, as discussed in the sections “Beam extraction window” and “Beam path out of vacuum”.

#### Beam extraction window

A window for beam extraction should not degrade its high tensile strength and radiation resistance, even for long irradiation time, and should minimise broadening of the beam size (negligible beam divergence) and energy distribution (very limited energy straggling). The use of Be, Al, Mica, polymer (Mylar, Al-Mylar, Kapton, Havar), Ti, Ni, Mo, Er, Zr, and Ta windows of different thicknesses has been reported [33–36], the 7.5  $\mu\text{m}$  Kapton foil being the most widely used. However, beam degradation induced by a 7.5- $\mu\text{m}$  Kapton window is not negligible, if micro-metric beam dimensions are required; for example, for a 3 MeV proton beam, just the 7.5  $\mu\text{m}$  Kapton foil, 2 mm downstream of the window, without taking into account the contribution of the atmosphere, induces a beam broadening of  $\sim 20 \mu\text{m}$  and an energy straggling of  $\sim 10 \text{ keV}$  (TRIM2008 calculation). In addition, the radiation hardness of the Kapton foil is not very satisfactory: even with

“rarefied” MeV proton beams (hundreds of microns spot size), kapton windows easily degrade under beam bombardment [3, 37]. This problem is increasingly relevant when beam dimensions are reduced, in order to obtain a microprobe, because the beam energy is released in smaller and smaller volumes. The dramatic increase of the damage density substantially shortens the life of the windows, which can last hours (or minutes) instead of weeks. In conclusion, none of the above mentioned windows is well suited to external microbeams.

State-of-art exit windows are ultra-thin (tens or hundreds of nanometres) silicon nitride ( $\text{Si}_3\text{N}_4$ ) membranes; the successful use of  $\text{Si}_3\text{N}_4$  windows with  $1 \times 1 \text{ mm}^2$  area, 50 nm thickness [38], and  $1 \times 1 \text{ mm}^2$  area, 100 nm thickness [28, 39, 40] has been reported; also  $2 \times 2 \text{ mm}^2$  (200 nm thick) and  $5 \times 5 \text{ mm}^2$  (500 nm thick) windows have been used when slight worsening of beam characteristic is endurable [19].

#### Beam path out of vacuum

In order to minimize also the beam spoil induced by the atmosphere, paths as short as possible in a light gas atmosphere, for example He or H instead of air, are normally mandatory, as can be deduced from Table 2, in which energy loss and straggling for 3 MeV protons are compared for typical window-to-target path lengths in He and air.

To give an example, at our external microbeam [19], the He atmosphere along the particle trajectories is guaranteed by a six-way system, one pipe for the beam path, one to reduce the absorption of low-energy X rays, one to cool the sample, and three to saturate the paths from sample to detectors of the backscattered and forward-scattered particles. Pipes are mounted on mini three-axis stages for fine aiming of the gas flow to the zone of interest.

The combined use of the 100 nm thick  $\text{Si}_3\text{N}_4$  windows and very short paths in light gases, most often He, enables very small probe dimensions to be achieved, even working out of vacuum. Table 3 summarises increases in probe dimensions for a 3-MeV proton beam after crossing the window (100 nm thick  $\text{Si}_3\text{N}_4$ ) and the ex-vacuo path; the strong reduction of beam diameter when substituting air with He is apparent.

**Table 2** Energy loss and straggling for 3-MeV protons in He and air, for typical window-to-target path lengths (TRIM2008 simulation)

Path length (mm) in atmosphere	Energy loss (keV)		Straggling ( $\sigma$ , keV)	
	Air	Helium	Air	Helium
2	28	6	4	1.5
3	40	8	5	2
4	54	10	6	2

**Table 3** Probe dimension increase for a 3-MeV proton beam after crossing an 100 nm thick Si<sub>3</sub>N<sub>4</sub> window and the external path (TRIM2008 simulation)

	External path length of the particles (mm)	FWHM (μm)		FW1/100 M (μm)	
		Air	He	Air	He
2		~6	~3.5	~25	~14
3		~11	~5	~50	~21
4		~18	~7	~74	~30

The spot size on the sample can be as small as few microns for 2–3 MeV protons, the size being further reduced if higher-energy protons are adopted [41].

### External IBA techniques

Detector setting is generally much easier ex-vacuo rather than in-vacuum, because the external set-up enables easy on-the-way adjustments of the detection geometry, such as adding a new detector, changing its orientation, or adjusting sample-to-detector distance, instances which may require installation of a new chamber, if working in vacuum.

When designing an external detection set-up, many efforts are made to minimise the distance crossed out of vacuum by the beam, without sacrificing the field of view of the detectors. To meet these requirements, it has been necessary to design structures for the beam exit snout [40–45], not obstructing the volume close to the beam-impact point on the sample. As a consequence, whereas with external milli-beams it is hard to use techniques different from PIXE/PIGE, with the advent of the external microbeams it has been possible to develop also techniques, for example external BS, ERDA, STIM, and IBIC, scarcely used, or not used at all in external milli-beam set-ups.

### PIXE

The energy straggling induced by the external beam path has a quite limited effect on quantitative analysis, because X-ray production cross sections are not highly dependent on beam energy and the He atmosphere along the beam path further reduces beam-energy indeterminacy. Because of the use of He atmosphere along the soft X-ray path from target to detector, PIXE is not affected by the limitations typical of the in-vacuum configuration. The main limit for lighter element detection arises from X-ray absorption in the sample itself, in the detector's entrance window, and in the detector dead layer, with absorption in the external path being practically negligible; for example, in a realistic low-energy X ray detector configuration, the transmission factors of the low-energy Na X-rays (~1 KeV) through a 5 cm long sample-to-target path in He (density  $\rho=0.167 \times 10^{-4}$  g cm<sup>-3</sup> and mass attenuation coefficient

$\mu/\rho=60.8$  cm<sup>2</sup> g<sup>-1</sup>) and a 7.5 μm thick Be window (density  $\rho=1.85$  g cm<sup>-3</sup>, mass attenuation coefficient  $\mu/\rho=604$  cm<sup>2</sup> g<sup>-1</sup>) [46] are respectively  $(I/I_0)_{\text{He}}=0.95$  and  $(I/I_0)_{\text{Be}}=0.43$ .

Problems arising from He permeation through the Be window of the Si(Li) detectors are widely discussed in Ref. [22]; as a matter of fact, a pump down of the cryostat volume enables removal of the pressure increase. To conclude, ex-vacuo and in-vacuum set-ups permit detection of low-energy X-rays, down to Na, with good sensitivity.

The external micro-PIXE technique has been the cornerstone of a wide project carried out since 1999 by the Spanish group of Seville for the non destructive study of the production of precious jewels in the south Iberian Peninsula, in the period between the 7th and the 2nd century BC (Refs. [30, 47] and references therein). The metallic alloys used for the many analysed jewels have been characterised, with the finding that the ancient goldsmiths used rich/very rich gold alloys (70–90% (w/w) Au, ~2.5% (w/w) Ag for the remaining part). For a subset of the analysed artefacts, it was also possible to propose a marker for provenance identification: the presence of Pa could possibly identify Punic jewels produced in the area of Cádiz. Finally, the soldering techniques were investigated and it was possible to find evidence of the systematic use of only two procedures, i.e. gold fusion and use of Ag/Cu alloy in the soldering points.

Also PIXE measurements with external α microbeams do not present particular difficulties, although α microbeams are not frequently used, because of the increase of beam divergence and energy straggling with respect to proton beams. A very good example is reported in Ref. [48] for the analysis of layered porcelain samples, constituted by a ~20 μm thick painted layer on a ~100 μm glaze, deposited over a porcelain bulk. α particles with energy of 2500 keV (~9 μm range in the decoration) were well suited to study just the decoration, without stimulating contributions from the glaze, whereas 8000 MeV α (40 μm range in the glaze) were the appropriate beam to analyze the glaze, without affecting the underneath porcelain. The external α-PIXE study disentangled the structure of the layers, in particular of the painted brush strokes, determining in a fully non-destructive way the pigment compositions, task not achievable with other techniques.

## PIGE

Because absorption is negligible practically for all  $\gamma$ -rays, external PIGE can take advantage of the ease of positioning detectors, with a possible relevant increase of the subtended solid angle. Quantitative PIGE analyses are carried out by integrating the  $\gamma$ -ray differential cross-sections along the beam path in the target;  $\gamma$ -ray production cross sections are often strongly dependent on beam energy [49], so, in principle, beam extraction, by broadening the energy distribution of the incoming particles, can make quantitative analyses less reliable. For thin/intermediate samples of unknown thickness and matrix composition, a possible strategy, typically followed in aerosol analysis, is to choose the energy of the incoming beam in such a way that the particle energy at the sample surface corresponds to the high-energy edge of a region where the cross-section is constant, this region being wider than the maximum energy loss of the beam in the target and of the corresponding energy straggling; the maximum energy loss in the sample must be measured in advance, to ascertain that the particle energy remains always inside the plateau region of the  $\gamma$ -ray cross section, independent on the local sample thickness [50–52]. When this strategy is possible, quantitative analysis can be performed by normalizing the  $\gamma$ -ray yield to the response obtained with thin standards under the same experimental conditions. For thick samples, in-vacuum and external PIGE are substantially equivalent, as the energy straggling in the external path induces negligible fluctuation in the total  $\gamma$ -ray yield from a thick target.

In Japan, in 2002, the microbeam group at JAERI, Takasaki, developed an external PIGE–PIXE set-up and started a project to study fluoride distribution and uptake in teeth [53]. The use of external proton beams enables avoidance of cracking on the teeth, preventing charging, and drastically lowering heating and drying. For this study, the elements of interest are F and Ca, studied by means of external PIGE ( $^{19}\text{F}(p, \alpha \gamma)^{16}\text{O}$  reaction) and external PIXE, respectively. After demonstrating the capability of the new system for characterising the distribution of fluorine in human teeth, the study has been extended to characterize the penetration into the tooth of F from thin layers of different F-releasing resins (these materials are under study for use for caries prevention, in conjunction with filling resins in dental restoration [40, 43, 54, 55]).

## IL

This technique was introduced quite recently and is still under development; results are very promising and have attracted substantial interest in the community [56–60]. Daylight, typically present when working out of a vacuum chamber, could in principle worsen the spectral sensitivity

of the technique, but this can be avoided by covering the experimental area with dark cloth. In normal applications, external IL does not seem to be disadvantaged compared with in-vacuum measurements. On the other hand, external IL is not feasible when target cooling is required, as for measurements with high spectral resolution.

Recently three independent studies exploited external IL for characterisation of pigments; in Ref. [17], external IL has been used to study formation of the dark spots induced by proton bombardment in IBA studies of pigments (dark spots are to be avoided when studying objects of art). During irradiation, IL + PIXE enabled identification of the impurities that act as recombination centres—Mn in calcite and dolomite, Pb in cerussite, and Cu in malachite and azurite; the modifications induced in the IL spectra by the proton damage are similar to those induced by X-ray and UV irradiation, both in the structure and in the peak position of the spectra. In Ref. [59], strong luminescence features were identified as fingerprints of the pigment identity, enabling, in some cases, discrimination of pigments of the same type but of different origins. In Refs [60, 61] a systematic study of the IL emitted by lapis lazuli is reported and criteria for identification of the provenance of the stone from the main historical sources were successfully proposed. On the basis of the results obtained, initial investigation of the provenance of the stone used for precious and delicate art objects of the Collezione Medicea has been carried out.

## BS

Information blur because of particle scattering along the external path is the main reason why BS is not commonly used out of vacuum. Nonetheless, when using standard detectors with energy resolution of the order of 10–15 keV, BS measurements are possible without noticeable worsening compared with in-vacuum measurements by:

1. installing ultra-thin windows for beam extraction (see the section “PIGE”);
2. adopting very short window-to-target distances, to limit the energy straggling *before* hitting the sample;
3. keeping the path of the scattered particles as short as possible, but anyway within a few millimetres;
4. exploiting He for the external path of the particles *before* and *after* the interaction;
5. using ultra-thin membranes (typically 1  $\mu\text{m}$  Al-Mylar or 100 nm thick  $\text{Si}_3\text{N}_4$ ) as entrance windows of the particle detectors.

This way, it is possible to minimise, and often make negligible, energy straggling originating from external configuration; as a consequence, because energy straggling is responsible for mass-resolution (i.e. the ability to discriminate similar target masses) worsening with respect

to in-vacuum operation, results obtained either ex-vacuo or in-vacuum may be practically the same. Two approaches are typically exploited for detector housing. In the former, the detector is hosted in the beam exit snout, so that the beam exit window is also the detector entrance window [62] (a recent implementation of this set-up is reported in Ref. [45]). This solution enables backscattered particles to be detected at large angles ( $170^\circ$  in the above mentioned configuration), so enhancing the mass resolution; interference with other detectors is minimized, so wide detection solid angles are achievable, e.g. by using annular detectors, as in Ref. [45]. High-quality external BS spectra have been obtained by the AGLAE group in Paris by following this approach for protons and, more noticeably, for  $\alpha$  particles; these spectra are practically indistinguishable from those obtained in vacuum under the same experimental conditions [45]. An elegant application of this external BS set-up, reported in Ref. [45], is a study of the black inlays decorating an ancient Japanese silver drop dispenser. The PIXE analysis identified the metallic alloy as a typical Shakudo alloy (Cu + a few percent of Ag and Au). The associated BS spectra indicate the presence of a copper compound, responsible of the characteristic black colour of the inlays, *over* the pure metallic bulk, as revealed by a small depletion of the Cu signal correlated with an O bump. The BS spectra also revealed evidence of the presence of a protective varnish, indicated by a C peak and by small, well defined steps in the Au and Ag contributions.

In the latter configuration [3, 19], the detector housing is separate from the beam exit snout; particle paths in the atmosphere after the interaction are typically longer, and backscattering angles wider than  $150\text{--}155^\circ$  are difficult to achieve. However, the scattering angle can be easily changed, if required, and beam scanning is not affected by the presence of the BS detector, as may be the case of the previous configuration. The external BS setup reported in Ref. [19] was used to characterise a SiC wafer with metal contacts. The external BS maps of the structure under investigation enabled understanding of the layer structure of the sample; the BS spectra extracted from proper sub-areas enabled determination of the composition and thickness of the layers.

The widely diffused and freeware SIMNRA simulation code [63] proved to be well fit to handle spectra obtained ex-vacuo, as it is able to take into account the beam exit window, the external paths of the incoming and back-scattered particles, the detector entrance window, and the particle path inside the detector housing.

## ERDA

The technique is very new and results are still scarce; in 2006 the AGLAE group proved the feasibility of ERDA measurements for hydrogen depth profiling ex-vacuo. In

that work, a 3-MeV  $^4\text{He}^{2+}$  static beam impinged at  $15^\circ$  to the specimen surface. Recoiled  $\text{H}^+$  ions were detected at a forward angle of  $30^\circ$ , with suppression of the beam particles scattered toward the detector by use of a “diffused” filter, obtained by setting the particle detector 84 mm far from the beam impact point on the sample, in an He atmosphere. External ERDA measurements were carried out also on quartz historical objects, in order to test the potential of ERDA for hydration-dating studies [64].

## IBIC

To the best of our knowledge, the first paper showing the use of external IBIC was presented in 2009 [38]. A 3,150-keV He beam was extracted in air through an  $\text{Si}_3\text{N}_4$  window, with 50 nm thickness and  $1\text{ mm}^2$  area, focused and raster scanned over the surface of a thin film CdS/CdTe solar cell. The beam spot on the sample was  $\sim 30\text{ }\mu\text{m}$ ,  $\sim 1\text{ mm}$  from the exit window. This work, while presenting the first IBIC characterisation of thin film solar cells, demonstrated the feasibility of external IBIC and its ability in investigating the electronic properties of such devices. The charge-collection efficiency of the solar cell was mapped and, in addition, the radiation hardness of the cell was characterised by continuous monitoring of the charge collection efficiency versus the ion fluence, from the perspective of space applications.

## STIM

In biomedical applications, STIM has been most often applied to the in-vacuum analysis of freeze-dried specimens [65]. External-beam analysis for biological and medical research has been reported since the mid-1970s, exploiting both milli and microbeams [66]. Quite surprisingly, external STIM for analysis of small living animals and cell imaging has been introduced rather recently, for example Refs. [44, 67, 68]. In 2001, at the nuclear microprobe of Bordeaux-Gradignan, the standard vacuum chamber for in-vacuum analysis was modified in order to accept a removable exit snout, supporting a standard  $\text{Si}_3\text{N}_4$  exit window. With this set-up, exploiting a 2.3-MeV proton beam with  $\sim 5\text{ }\mu\text{m}$  spatial resolution, energy loss STIM images of living cultured cells were reported. By use of the external STIM images, it was possible to identify sub-cellular ultra-structures. The combination of STIM and IBA analysis with external beam microprobes was suggested as a qualitative improvement for trace element studies in living cells.

## Charge normalisation in external set-ups

To carry out quantitative analysis it is essential the measure of the charge falling on the target. In vacuum, when

studying thin samples, the beam charge is integrated by using a Faraday cup behind the target; for thick samples, it is normally collected directly on the object under examination, most often applying a positive bias to prevent electron loss.

In external applications, direct charge integration is not as easy as in vacuum, because electrons created by the beam along the external path and in the target itself do not always recombine with the corresponding positive ions and may be discharged to ground, leading to incorrect charge determination. Adding a positive bias to prevent electron loss does not enable proper charge integration out of vacuum, because a current would always be measured, even in absence of the beam (atmosphere = plenty of free charge carriers).

For thin targets, proper direct charge integration in external applications with a Faraday cup is possible by using long and narrow Faraday cups, as close as possible to the sample to minimise electron loss, and high beam intensities, at least on the nA scale, because discrepancies between measured and actual charge values decrease with increasing beam intensity [69]. For thick targets, direct charge integration on the sample itself is normally unreliable (see Ref. [70] for a review of the charge measurement in external applications).

Alternative systems rely on its indirect measurement and exploit detection of the:

1. radiation induced by the incoming particles in a target, over which the beam is periodically deflected [45];
2. X-rays emitted or beam particles backscattered by the exit window [3, 19];
3. particles backscattered by the sample itself; in this case a simultaneous BS analysis of the sample has to be carried out and the charge is deduced from the area of the BS spectrum [41];
4. X-ray emitted or beam particles backscattered from a chopper periodically intercepting the beam [21, 69];
5. scattered particles, visible light, or X-rays emitted by the gas molecules between the exit window and target [36, 71–73].

With external microbeams, the first three methods, only, are typically exploited; the other normalisation techniques seem infeasible, because of the very compact detection geometry, the extremely short window-to-target distance, and the He atmosphere.

## Conclusions

External microbeams have made available both the favourable aspects of external set-ups and high resolution probes, the dimensions of which can be well in the micron range;

for thick targets the spatial resolution achievable ex-vacuo can be equivalent to that achievable in-vacuum.

Besides the already existing external PIXE and PIGE, out-of-vacuum microbeams have enabled the development of external BS, ERDA, STIM, and IBIC, scarcely used or not applied previously.

Because of the combined use ex-vacuo of scanning microprobes and IBA techniques in external applications, it is now possible to obtain a rich insight into samples of interest for a wide set of sciences with high spatial resolution and with strongly reduced or even suppressed damage to the samples, thus enabling the study of samples characterised by low radiation resistance or easily damaged if put in vacuum.

**Acknowledgements** The author is deeply indebted to Dr M. Massi and Dr P. Olivero for many fruitful discussions and suggestions. This work was carried out in the framework of the experiment “FARE” of the Italian National Institute of Nuclear Physics.

## References

1. Jolly RK, Randers-Pehrson G, Gupta SK, Buckle DC, Aceto H, Proc Third Conf. on Applications of Small Accelerators, Denton, Texas, 1974, NTIS Report CONF741040-PI
2. Seaman GC, Shane KC (1975) Nucl Instrum Method B 126:473–474
3. Calligaro T, Dran J-C, Ioannidou E, Moignard B, Pichon L, Salomon J (2000) Nucl Instrum Method B 161–163:328–333
4. Watt F, Grime GW (1987) High-energy ion microbeams. Adam Hilger, Bristol
5. Cookson JA (1979) Nucl Instrum Method 165:477–508
6. Hamada N, Ni M, Funayama T, Sakashita T, Kobayashi Y (2008) Mutat Res 639:35–44
7. Gerardi S (2009) J Radiat Res 50(Suppl):A13–A20
8. Meijer J, Stephan A, Adamczewski J, Reken H, Bukow HH, Rolfs C (1995) Nucl Instrum Method B 99:423–426
9. Ryan CG, Jamieson DN (1999) Nucl Instrum Method B 158:997–1066
10. Dollinger G, Datzmann G, Hauptner A, Hertenberger R, Körner H-J, Reichart P, Volckaerts B (2003) Nucl Instrum Method B 210:6–13
11. Randers-Pehrson G, Johnson GW, Marino SA, Xu Y, Dymnikov AD, Brenner DJ (2009) Nucl Instrum Method A 609:294–299
12. Merchant MJ, Grime GW, Kirkby KJ, Webb R (2007) Nucl Instrum Method B 260:8–14
13. Watt F, van Kan JA, Rajta I, Bettiol AA, Choo TF, Breese MBH, Osipowicz T (2003) Nucl Instrum Method B 210:14–20
14. Grime GW, Dawson M, Marsh M, McArthur JD, Watt F (1991) Nucl Instrum Method B 54:353–362
15. Moliere G (1948) Z Naturforsch 3a:78
16. <http://www.srim.org/>
17. Enguita O, Fernandez-Jimenez MT, Garcia G, Climent-Font A, Calderon T, Grime GW (2004) Nucl Instrum Method B 219–220:384–388
18. Remazeilles C, Quillet V, Calligaro T, Dran J-C, Pichon L, Salomon J (2001) Nucl Instrum Method B 181:681–687
19. Giuntini L, Massi M, Calusi S (2007) Nucl Instrum Method A 576:266–273
20. Grassi N, Giuntini L, Massi M, Mandò PA (2007) Nucl Instrum Method B 256:712–718



21. Chiari M, Del Carmine P, Garcia Orellana I, Lucarelli F, Nava S, Paperetti L (2006) *Nucl Instrum Method B* 249:584–587
22. Mandò PA (1994) *Nucl Instrum Method B* 85:815–823
23. Calligaro T, Dran J-C, Hamon H, Moignard B, Salomon J (1998) *Nucl Instrum Method B* 136–138:339–343
24. Kirby BJ, Legge GJF (1991) *Nucl Instrum Method B* 54:98–100
25. Randers-Pehrson G, Johnson GW, Marino SA, Xua Y, Dymnikov AD, Brenner DJ (2009) *Nucl Instrum Method A* 609:294–299
26. Ortega R, Devès G, Moretto Ph (2001) *Nucl Instrum Method B* 181:475–479
27. Feng H, Yu Z, Chu PK (2006) *Mater Sci Eng R* 54:49–120
28. Dran J-C, Salomon J, Calligaro T, Walter P (2004) *Nucl Instrum Method B* 219–220:7–15
29. Mandò PA (2005) *Nucl Phys A* 751:393–408
30. Respaldiza MA, Ager FJ, Carmona A, Ferrer J, García-León M, García-López J, García-Orellana I, Gómez-Tubío B, Morilla Y, Ontalba MA, Ortega-Feliu I (2008) *Nucl Instrum Method B* 266:2105–2109
31. Perea A, Climent-Font A, Fernández-Jiménez M, Enguita O, Gutiérrez PC, Calusi S, Migliori A, Montero I (2006) *Nucl Instrum Method B* 249:638–641
32. Migliori A, Grassi N, Mandò PA (2008) *Nucl Instrum Method B* 266:2339–2342
33. Räsänen J, Anttila A (1982) *Nucl Instrum Method* 196:489–492
34. Del Carmine P, Lucarelli F, Mandò PA, Pecchioli A (1993) *Nucl Instrum Method B* 75:480
35. Calligaro T, McArthur JD, Salomon J (1996) *Nucl Instrum Method B* 109:125
36. Neelmeijer C, Wagner W, Schramm HP (1996) *Nucl Instrum Method B* 118:338–345
37. Kinomura A, Mokuno Y, Chayahara A, Tsubouchi N, Horino Y (2003) *Nucl Instrum Method B* 210:75–78
38. Colombo E, Bosio A, Calusi S, Giuntini L, Lo Giudice A, Manfredotti C, Massi M, Olivero P, Romeo A, Romeo N, Vittone E (2009) *Nucl Instrum Method B* 267:2181–2184
39. Lefèvre HW, Schofield RMS, Bench GS, Legge GJF (1991) *Nucl Instrum Method B* 54:363–370
40. Yasuda K, Hai VH, Nomachi M, Sugaya Y, Yamamoto H (2007) *Nucl Instrum Method B* 260:207–212
41. Grime GW, Abraham MH, Marsh MA (2001) *Nucl Instrum Method B* 181:66–70
42. Mathis F, Moignard B, Pichon L, Dubreuil O, Salomon J (2005) *Nucl Instrum Method B* 240:532–538
43. Komatsu H, Yamamoto H, Nomachi M, Yasuda K, Matsuda Y, Murata Y, Kijimura T, Sano H, Sakai T, Kamiya T (2007) *Nucl Instrum Method B* 260:201–206
44. Nilsson C, Petriconi S, Reinert T, Butz T (2007) *Nucl Instrum Method B* 260:71–76
45. Salomon J, Dran J-C, Guillou T, Moignard B, Pichon L, Walter P, Mathis F (2008) *Nucl Instrum Method B* 266:2273–2278
46. <http://physics.nist.gov/PhysRefData/XrayMassCoef/cover.html>
47. Ortega-Feliu I, Gómez-Tubío B, Ontalba Salamanca MÁ, Respaldiza MÁ, de la Bandera ML, Ovejero Zappino G (2007) *Nucl Instrum Method B* 260:329–335
48. Zucchiatti A, Pascual C, Ynsa MD, Castelli L, Recio P, Criado E, Valle FJ, Climent-Font A (2008) *J Eur Ceram Soc* 28:757–762
49. <http://www-nds.iaea.org/iband1/>
50. Boni C, Cereda E, Braga Marcazzan GM, De Tomasi V (1988) *Nucl Instrum Method* 35:80
51. Lucarelli F, Mandò PA, Nava S, Prati P, Zucchiatti A (2004) *J Air Waste Manage Assoc* 54:1372–1382
52. Calzolari G, Chiari M, Lucarelli F, Nava S, Portarena S (2010) *Nucl Instrum Method B* 268:1540–1545
53. Sakai T, Kamiya T, Oikawa M, Sato T, Tanaka A, Ishii K (2002) *Nucl Instrum Method B* 190:271–275
54. Yamamoto H, Nomachi M, Yasuda K, Iwami Y, Ebisu S, Komatsu H, Sakai T, Kamiya T (2007) *Nucl Instrum Method B* 260:194–200
55. Komatsu H, Yamamoto H, Nomachi M, Yasuda K, Matsuda Y, Kinugawa M, Kijimura T, Sano H, Satou T, Oikawa S, Kamiya T (2009) *Nucl Instrum Method B* 267:2136–2139
56. Spemann D, Jankuhn St, Vogt J, Butz T (2000) *Nucl Instrum Method B* 161–163:867–871
57. Sha Y, Zhang P, Wang G, Zhang X, Wang X (2002) *Nucl Instrum Method B* 189:408–411
58. Enguita O, Calderón T, Fernández-Jiménez MT, Beneitez P, Millan A, García G (2004) *Nucl Instrum Method B* 219–220:53–56
59. Quaranta A, Salomon J, Dran J-C, Tonezzer M, Della Mea G (2007) *Nucl Instrum Method B* 254:289–294
60. Calusi S, Colombo E, Giuntini L, Lo Giudice A, Manfredotti C, Massi M, Pratesi G, Vittone E (2008) *Nucl Instrum Method B* 266:2306–2310
61. Lo Giudice A, Re A, Calusi S, Giuntini L, Massi M, Olivero P, Pratesi G, Albonico M, Conz E (2009) *Anal Bioanal Chem* 395:2211–2217
62. Doyle BL (1983) *Nucl Instrum Method* 218:29–32
63. <http://www.simnra.com/>
64. Reiche I, Castaing J, Calligaro T, Salomon J, Aucouturier M, Reinholz U, Weise H-P (2006) *Nucl Instrum Method B* 249:608–611
65. Llabador Y, Moretto Ph (1998) *Nuclear microprobes in the life sciences*. World Scientific, Singapore
66. Williams ET (1984) *Nucl Instrum Method B* 3:211
67. Sugimoto A, Ishii K, Matsuyama S, Satoh T, Gotoh K, Yamazaki H, Akama C, Sato M, Sakai T, Kamiya T, Oikawa M, Saido M, Tanaka R (1999) *Int J PIXE* 9:151–160
68. Kamiya T, Sakai T, Oikawa M, Satoh T, Ishii K, Sugimoto A, Matsuyama S (1999) *Int J PIXE* 9:217–225
69. Chiari M, Migliori A, Mandò PA (2002) *Nucl Instrum Method B* 188:162–165
70. Šmit Ž, Uršič M, Pelicon P, Trček-Pečak T, Šeme B, Smrekar A, Langus I, Nemec I, Kavkler K (2008) *Nucl Instrum Method B* 266:2047–2059
71. Hietel B, Menzel N, Wittmaack K (1996) *Nucl Instrum Method B* 109/110:139–143
72. Lill JO (1999) *Nucl Instrum Method B* 150:114–117
73. Budnar M, Uršič M, Simčič J, Pelicon P, Kolar J, Šelih VS, Strlič M (2006) *Nucl Instrum Method B* 243:407–416